A Two-Season Impact Study of Four Satellite Data Types and Rawinsonde Data in the NCEP Global Data Assimilation System

TOM H. ZAPOTOCNY

Cooperative Institute for Meteorological Satellite Studies, and Space Science and Engineering Center, University of Wisconsin—Madison, Madison, Wisconsin, and Joint Center for Satellite Data Assimilation, Camp Springs, Maryland

JAMES A. JUNG

Cooperative Institute for Meteorological Satellite Studies, University of Wisconsin—Madison, Madison, Wisconsin, and Joint Center for Satellite Data Assimilation, Camp Springs, Maryland

JOHN F. LE MARSHALL

University of Maryland, College Park, College Park, and Joint Center for Satellite Data Assimilation, Camp Springs, Maryland

RUSS E. TREADON

National Centers for Environmental Prediction, and Joint Center for Satellite Data Assimilation, Camp Springs, Maryland

(Manuscript received 29 January 2007, in final form 9 May 2007)

ABSTRACT

Extended-length observing system experiments (OSEs) during two seasons are used to quantify the contributions made to forecast quality by conventional rawinsonde data and four types of remotely sensed satellite data. The impact is measured by comparing the analysis and forecast results from an assimilation–forecast system using all data types with those excluding a particular observing system. The impact of the particular observing system is assessed by comparing the forecast results over extended periods. For these observing system experiments, forecast results are compared through 168 h for periods covering more than a month during both the summer and winter seasons of each hemisphere. The assimilation–forecast system used for these experiments is the National Centers for Environmental Prediction (NCEP) Global Data Assimilation System (GDAS) and the Global Forecast System (GFS). The case studies chosen consist of periods during January–February 2003 and August–September 2003. During these periods, a T254L64 layer version of NCEP's global spectral model was used. The control run utilized all data types routinely assimilated in the GDAS. The experimental runs individually denied data from the Advanced Microwave Sounding Unit (AMSU), the High-Resolution Infrared Radiation Sounder (HIRS), geostationary satellite atmospheric motion vectors (GEO winds), in situ rawinsondes (raobs), and surface winds derived from the Quick Scatterometer (QuikSCAT). Differences between the control and denial experiment forecasts are accumulated over the two 45-day periods and are analyzed to demonstrate the impact of these data types. Anomaly correlations (ACs), forecast impacts (FIs), and hurricane track forecasts are evaluated for all experimental runs during both seasons. The anomaly correlations used the standard NCEP software suite and are partitioned into subsections covering the polar caps (60°–90°) and midlatitudes (20°–80°) of each hemisphere and the tropical region (20°N–20°S). Anomaly correlations of geopotential heights are shown at several pressure levels in the polar regions and midlatitudes. The root-mean-square error (RMSE) for 850- and 200-hPa wind vector differences are shown for the tropical region. The geographical distributions of forecast impacts on geopotential heights are also examined. The influence these data types have on tropical cyclone track forecasts are shown for both the Atlantic and Pacific basins and again are computed using standard algorithms developed and maintained at NCEP. The results demonstrate a positive impact from all data types with AMSU and rawinsonde data providing the largest anomaly correlation improvements in all zonal regions examined. Smaller forecast improvements are noticed from each of the other data types. In the Atlantic basin, each of the four satellite data types provides nearly equal improvement to the tropical cyclone track forecasts; however, GEO winds provide the largest improvement to track forecasts in the Pacific basin.

Corresponding author address: James A. Jung, NOAA Science Center, 5200 Auth Rd., Camp Springs, MD 20746-4304.
E-mail: jim.jung@noaa.gov

DOI: 10.1175/2007WAF2007010.1

TABLE 1. Satellite data assimilated within the NCEP GDAS for this study.

HIRS sounder radiances	TRMM precipitation rates
AMSU-A sounder radiances	*European Remote Sensing Satellite-2* (*ERS-2*) ocean surface wind vectors
AMSU-B sounder radiances	QuikSCAT ocean surface wind vectors
GOES sounder radiances	AVHRR SSTs
GOES, GMS, and *Meteosat* wind vectors	AVHRR vegetation fraction
GOES precipitation rate	AVHRR surface type
SSM/I ocean surface wind speed	Multisatellite sea ice
SSM/I precipitation rate	SBUV/2 ozone profile and total ozone

1. Introduction

A diagnostic evaluation of five data types being used by the National Centers for Environmental Prediction (NCEP) operational Global Data Assimilation System (GDAS) is produced in this study. These types of studies help realize the full impact of some of the numerous data sources available today. All types of remotely sensed data are prime examples of such data requiring diagnostic study of their impact in both regional and global models. If these types of experiments are not conducted, the influence of each data type will never be fully understood or identified.

A unique aspect of this work, afforded by the Joint Center for Satellite Data Assimilation (JCSDA) and NCEP, was the ability to conduct impact studies at the operational resolution of the time. Until recently, limited computational resources required that studies covering several seasons be completed at reduced spatial and vertical resolutions. This limitation restricted the conclusions that could be reached about the impact of data types at the operational resolutions.

Similar studies are also being undertaken for data available from a number of new instruments. Such instruments include, but are not limited to, atmospheric motion vector (AMV) algorithm data from the Moderate Resolution Imaging Spectroradiometer (MODIS), Atmospheric Infrared Radiometer (AIRS) radiances, and ocean surface wind vector measurements using WindSat.

This report is a follow-on to Zapotocny et al. (2007), which investigated the forecast impact of all conventional in situ data as well as all remotely sensed satellite data used in GDAS. In this work the five data types composing the majority of the observations in Zapotocny et al. (2007) are individually denied (excluded from the operational forecast system). Rawinsonde data are denied because they are a key contributor to forecast quality from conventional data. Remotely sensed satellite data denied in this study include the Advanced Microwave Sounding Unit (AMSU) data, High-Resolution Infrared Radiation Sounder (HIRS) data, geostationary satellite atmospheric motion vectors (GEO winds) data from both the National Oceanic and Atmospheric Administration (NOAA) Geostationary Operational Environmental Satellite (GOES) and the Japan Geostationary Meteorological Satellite (GMS), and Quick Scatterometer (QuikSCAT) surface wind data.

The work in this manuscript is similar to observing system experiments (OSEs) conducted with the European Centre for Medium-Range Weather Forecasts (ECMWF) Global Model by Kelly (1997) and is complementary to Zapotocny et al. (2000, 2002, 2005a,b), who explored forecast impacts from satellite and in situ data in the NCEP regional model.

The paper is structured as follows: section 2 briefly outlines which GDAS–GFS version was used for this study. Section 3 discusses the diagnostics used to evaluate the anomaly correlation and forecast impacts. Section 4 presents the anomaly correlation results in tropical, midlatitude, and polar regions for all data types investigated through 7 days of model forecasts. Geographic distributions of forecast impacts are also presented for the denied data types as is an examination of the impacts of these data types on tropical cyclone track forecast accuracy. The results are summarized in section 5.

2. The model and assimilation systems

Most of the details concerning the assimilation system and details about the version of the forecast model used in this work are available in Zapotocny et al. (2007, section 2). As such, only a very brief description is offered here. For these denial experiments, the full operational database of conventional and satellite data was used, including the real-time data cutoff constraints for the early and late assimilation cycles produced at NCEP.

The assimilated satellite data used in this work are shown in Table 1 and include operational Advanced Television Infrared Observation Satellite (TIROS-N) (Reale 1995) Operational Vertical Sounder (TOVS) (Smith et al. 1979) radiances from HIRS, the Microwave Sounding Unit (MSU) (Spencer and Christy 1992), AMSU-A and AMSU-B sensors (NOAA 2005), ozone information from the Solar Backscatter Ultra-

TABLE 2. In situ data assimilated within the NCEP GDAS for this study.

Mass observations	Wind observations
Rawinsonde temperature and humidity	Rawinsonde u and v
Aircraft reports (AIREP) and pilot reports (PIREP)	AIREP and PIREP aircraft u and v
Aircraft-to-satellite data relay (ASDAR) aircraft temperatures temperatures	ASDAR aircraft u and v
Flight-level reconnaissance and dropsonde temperature, humidity, and station pressure	Flight-level reconnaissance and dropsonde u and v
Meteorological Data Collection and Reporting System (MDCARS) aircraft temperatures	MDCARS aircraft u and v
Surface land synoptic and aviation routine weather report (METAR) temperature, humidity, and station pressure	Surface marine ship, buoy, and C-Man u and v
Ship temperature, humidity, and station pressure	Surface land synoptic and METAR u and v
	Wind profiler u and v
	Next Generation Weather Radar (NEXRAD) vertical azimuth display u and v
	Pibal u and v

violet (SBUV) sensors (Miller et al. 1997), Defense Meteorological Satellite Program (DMSP) Special Sensor Microwave Imager (SSM/I) surface wind speed (Alishouse et al. 1990), derived surface winds from QuikSCAT (Yu and McPherson 1984), and AMVs from geostationary satellites (Velden et al. 1997; Menzel et al. 1998).

The assimilated in situ data used in this work are displayed in Table 2 and include rawinsonde temperature, specific humidity, and wind components; aircraft observations of wind and temperature; land surface reports of surface pressure; and oceanic reports of surface pressure, temperature, horizontal wind, and specific humidity. Keyser (2001a,b, 2003) provide an excellent overview of data types provided to NCEP on a daily basis and used operationally for the experiments of this study.

The assimilation and forecast methodologies were consistent with NCEP's operational system and are explained in Zapotocny et al. (2007). The only difference is that this work examines the forecast from 0000 UTC, whereas NCEP operations runs forecasts at 0000, 0600, 1200, and 1800 UTC. Our reduction in horizontal and vertical resolutions from T254L64 initially to T170L42 at 84 h and T126L28 at 180 h is also consistent with NCEP operations of the time.

The versions of the Global Spectral Model (Kanamitsu et al. 1991) and GDAS (Derber et al. 1991; Parrish and Derber 1992) used in this work are identical to the versions used in Zapotocny et al. (2007, sections 2a and 2b). Likewise, the experimental design, including the time periods used; diagnostics; and methodology for display are all the same as used in Zapotocny et al. (2007, section 3). For completeness, a log of changes to the Global Spectral Model since 1991 is available online (http://www.emc.ncep.noaa.gov/gmb/STATS/html/model_changes.html). Likewise, a log of changes to the assimilation system is also available online (http://www.emc.ncep.noaa.gov/gmb/gdas/). Finally, the results of this paper and the previous work were all computed and archived at NCEP on the research and development machine of the time.

3. Experimental design

Diagnostics presented here include statistics commonly used at NCEP and other NWP centers. The computation of all anomaly correlations for forecasts produced by the GFS were completed using code developed and maintained at NCEP. NCEP (NWS 2007) provides a clear description of the method of computation, while Lahoz (1999) presents an overall description of the use of the anomaly correlation. The fields being evaluated, which are truncated to include spectral wavenumbers 1–20, are examined in the zonal bands 60°–90° (hereafter referred to as the polar region) and 20°–80° of each hemisphere and in the tropical region within 20° of the equator (20°N–20°S).

The NCEP–National Center for Atmospheric Research (NCAR) reanalysis fields (Kistler et al. 2001) are used for the climate component of the anomaly correlations. This reanalysis was run at a resolution of T62L28 with the output grids transformed from spectral to pressure coordinates and reduced to 2.5° × 2.5° horizontal resolution and to rawinsonde mandatory levels. To calculate anomaly correlations, the output from the control and the five experiments were also transformed to pressure coordinates and reduced to 2.5° × 2.5° horizontal resolution using the NCEP postprocessor. Reducing the T254L64 simulations of this study to a 2.5° × 2.5° horizontal resolution is the standard recommended by the WMO (1999) and traditionally used at NCEP for evaluation of their anomaly correlations. To evaluate the anomaly correlation at the full horizontal resolution of this experiment requires a matching climate field to be available. Climate fields at 55-km resolution are not available from NCEP or from the 40-yr ECMWF Reanalysis (ERA-40) project (Uppala et al. 2005).

Another diagnostic used here is to evaluate the fore-

cast impact (FI), as discussed further by Zapotocny et al. (2005a, 2007). For this study, a series of two-dimensional FI results are presented as the positive–negative impact provided by the denial of a particular data type. The geographic distributions of FI shown in section 4b for a specific pressure level are evaluated using

$$\mathrm{FI}(x, y) = 100 \times \left\{ \left[\sqrt{\frac{\sum_{i=1}^{N} (D_i - A_i)^2}{N}} - \sqrt{\frac{\sum_{i=1}^{N} (C_i - A_i)^2}{N}} \right] \Bigg/ \sqrt{\frac{\sum_{i=1}^{N} (C_i - A_i)^2}{N}} \right\}. \quad (1)$$

The variables C and D are the control and denied forecasts, respectively. The variable A is the 0-h GDAS control analysis containing all data types, which is valid at the same time as the forecasts. Here, N is the number of diagnostic days. All FI diagnostics were computed from the $1^\circ \times 1^\circ$ grids generated by NCEP's postprocessing package.

The first term on the right side enclosed by parentheses in (1) can be considered the error in the denied experiment. The second term enclosed by parentheses in (1) can be considered the error in the control forecast. Dividing by the error of the control forecast normalizes the results. Multiplying by 100 provides a percent improvement–degradation with respect to the RMS error of the control forecast. A positive forecast impact means the forecast compares more favorably to its corresponding analysis with the data type excluded.

All diagnostics exclude the first 15 days of each seasonal time period. This delay in evaluating the statistics allows for the impact of the denied data to be removed from the model initial conditions. Excluding the first 15 days reduces the two seasonal windows to 32 and 37 days for the Northern Hemisphere winter and summer, respectively. The forecast diagnostics for this paper were terminated at 168 h to concentrate on the shorter-term forecast impacts.

4. Results

The impacts of the four individual satellite data types and the rawinsonde data on the quality of the forecasts made by the GFS for two time periods are now explored in detail. The first time period covers 15 January–15 February 2003 and the second covers 15 August–20 September 2003. The selection of these time periods enables the diagnostics to capture both summer and winter seasons in each hemisphere. The Northern Hemisphere summer period is shifted and slightly extended toward the autumn season to capture tropical cyclone events in that hemisphere (section 4c). The fields diagnosed consist of geopotential heights, wind vector differences, and hurricane track forecast accuracy. Underground grid points on isobaric surfaces intersecting the earth's surface are not included in the evaluations.

a. Anomaly correlations

Figure 1 presents the anomaly correlations for day 5 from the control simulation and five experiments during January–February 2003 and August–September 2003. The five experiments involve denying AMSU (No_AMSU), HIRS (No_HIRS), geostationary atmospheric motion vectors (No_GEO Wind), rawinsondes (No_RAOB), and QuikSCAT surface winds (No_QSCAT) data for the entire period of the experiment. The fields diagnosed include the 1000- and 500-hPa geopotential height anomaly correlations for midlatitudes in both hemispheres and time periods (Figs. 1a and 1d); the 500- and 850-hPa geopotential height anomaly correlations for the Northern Hemisphere polar regions and the 500- and 700-hPa geopotential height anomaly correlations for the Southern Hemisphere polar regions (Figs. 1b and 1e); and 200- and 850-hPa vector and speed anomaly correlations for the tropics (Figs. 1c and 1f). (Note the vertical scale of the values in Fig. 1c and 1f relative to the other four panels.) The anomaly correlations are higher in the extratropics and the poles for geopotential height than for wind-related fields in the tropics. This is an expected result considering the large-scale nature of geopotential heights relative to wind fields.

It is expected that the control simulation would have the highest anomaly correlations and the denial experiments would be lower. This would imply that the addition of the data improved forecast quality. However, examination of the results in Fig. 1 indicates that only the No_AMSU and No_RAOB experiments satisfy this condition for nearly all fields presented. The other data types have occurrences of the control and denied simulations either tying or the denied simulation producing a slightly higher anomaly correlation than the control simulation. Another point is that all of the tropical anomaly correlations are approximately 0.15 worse in August–September than they are in January–February. This could be related to the broader expanse of deep tropical convection in August–September than in January–February.

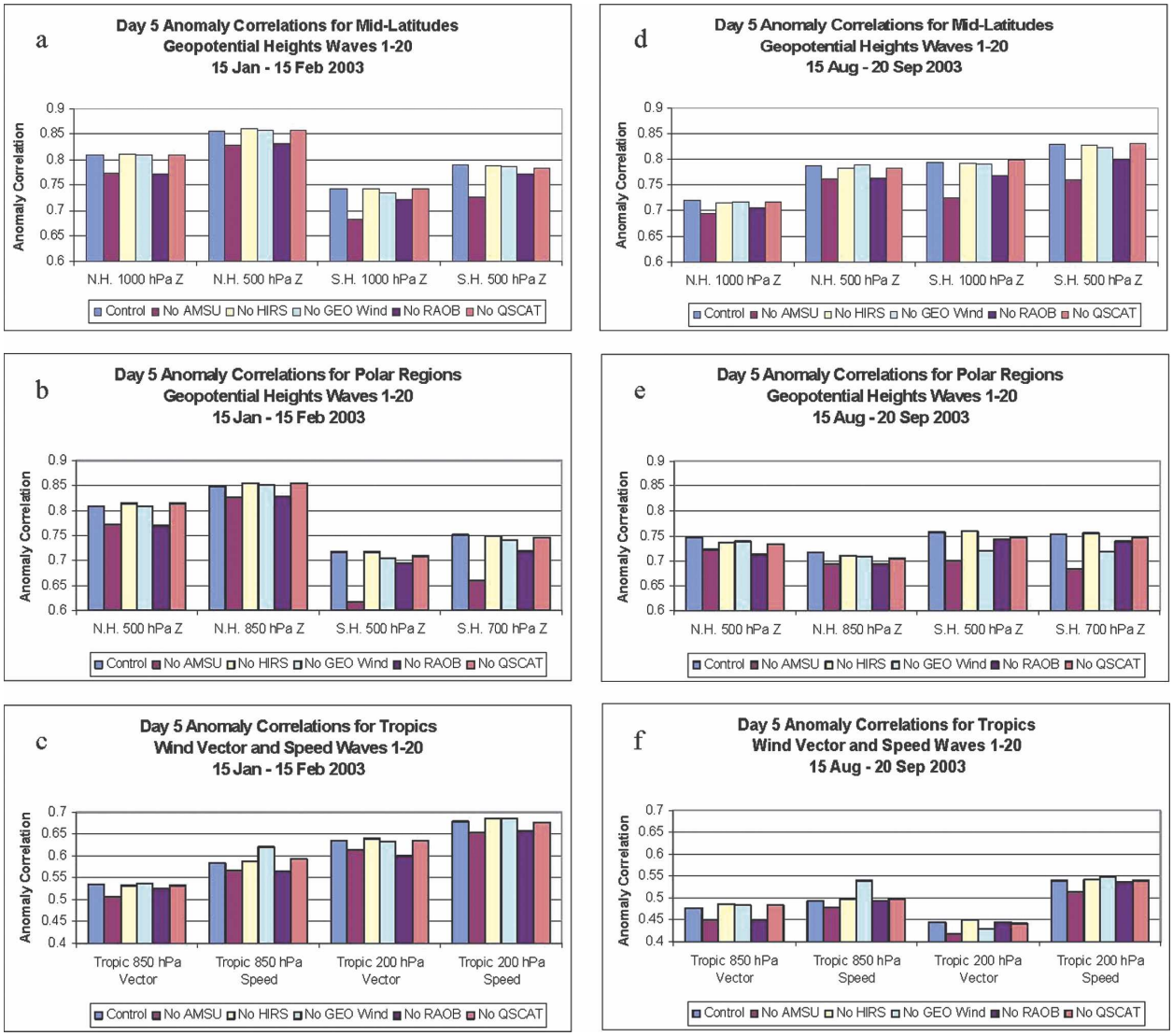

FIG. 1. The day-5 anomaly correlations for waves 1–20 for the (a), (d) midlatitudes; (b), (e) polar regions; and (c), (f) tropics. Experiments shown for each term include, from left to right, the control simulation and denials of AMSU, HIRS, GEO winds, rawinsondes, and QuikSCAT. Shown are the (left) 15 Jan–15 Feb 2003 and (right) 15 Aug–20 Sep results. Note the different vertical scale in (c), (f).

Figure 2 depicts the 20°–80°Northern and Southern Hemisphere 500-hPa geopotential height day-0–7 anomaly correlation die-off curves for the control simulation and the five denial experiments of this study during January–February 2003. The dark blue line is the control simulation, which closely replicates NCEP operations and includes all data routinely used by the GDAS. The magenta line is the anomaly correlation diagnosed from the simulations when removing the specific data. In this denial experiment, the larger the separation between the anomaly correlations for the denied and control experiments, the greater the importance of the removed data to the quality of the simulation. Note also, it is generally accepted that a forecast with an anomaly correlation of 0.6 or greater provides a useful forecast.

Examining the control versus No_AMSU 500-hPa Northern Hemisphere geopotential height anomaly correlation (Fig. 2a) indicates that the control experiment anomaly correlation is consistently higher after day 1. The day-5 control anomaly correlation is just greater than 0.85 while the No_AMSU anomaly correlation is approximately 0.825. This spread continues to grow between days 5 and 7. The difference between the control simulation and the No_AMSU experiment is even more noticeable in the Southern Hemisphere dur-

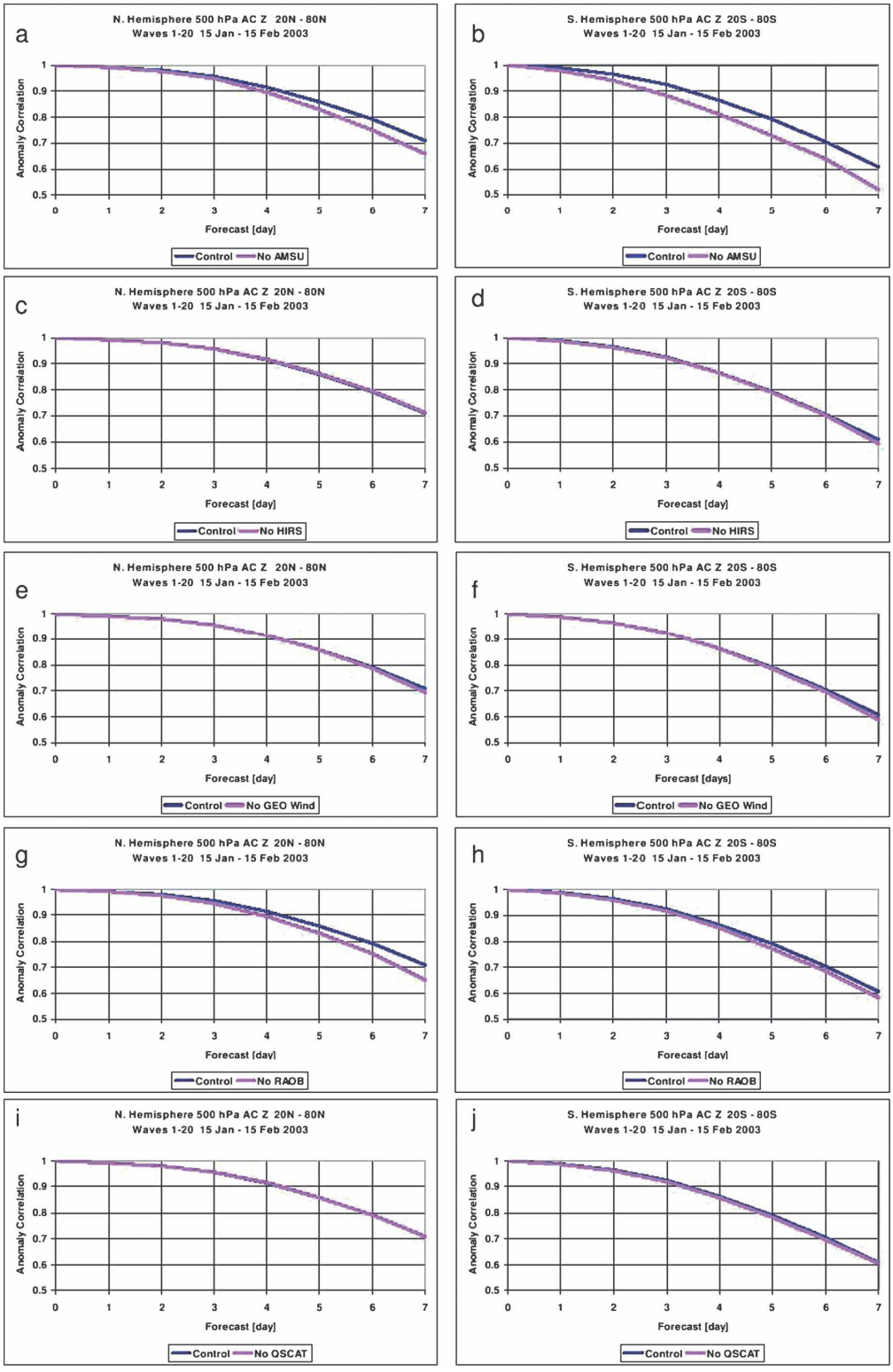

FIG. 2. The 15 Jan–15 Feb 2003 day-0–7 500-hPa geopotential height die-off curves for the control and five denial experiments. Shown are the (left) Northern Hemisphere and (right) Southern Hemisphere results.

ing January–February 2003 (Fig. 2b). In this hemisphere the day-5 anomaly correlation difference between the control simulation and AMSU denial is approximately 0.075, with even larger differences at day 7.

A possible explanation for the No_AMSU experiment having such a large impact could be due to the AMSU coverage and its insensitivity to clouds. With three satellites having AMSU sensors, the coverage for each assimilation cycle is almost global. The AMSU is also able to look through nonprecipitating clouds. These two features allow AMSU radiances to provide vertical profiles of temperature and moisture information almost globally for every assimilation cycle.

Figures 2c–j present the 20°–80°Northern and Southern Hemisphere anomaly correlations for the remaining four denials completed in this study in the same order as presented in Fig. 1. Cumulatively examining these four data types, along with the results just shown in Figs. 2a and 2b, indicates that denying the AMSU data had the largest impact to forecast quality for most time periods, in both hemispheres and most days. The impact of the denial of rawinsonde data is almost as large in the Northern Hemisphere (cf. Figs. 2a and 2g). The remaining three experiments (No_HIRS, No_GEO_Wind, and No_QSCAT) all produced minimal improvements at midlatitudes in each hemisphere during January–February 2003. However, none of the data types incorporated into the NCEP GDAS–GFS system resulted in a negative impact when time averaged over these particular seasons.

Figure 3 presents results for the same denial experiments and fields as shown Fig. 2, except that the time period is 15 August–20 September 2003. Overall, these results are very similar to their January–February 2003 counterparts. The No_AMSU and No_RAOB experiments are again considerably worse than the control simulation when the data are removed from the assimilation system. Comparing the No_AMSU and No_RAOB results, it is clear that the rawinsonde data are more important in the Northern Hemisphere than the AMSU data (cf. Figs. 3a and 3g), but the AMSU data are more important in the Southern Hemisphere (cf. Figs. 3b and 3h). Because there are considerably less rawinsondes in the Southern Hemisphere, the AMSU should play a larger role in the forecast quality. This is consistent with the Zapotocny et al. (2007) results. Again, the overall impact of all data is positive and while often appearing small it is found to remove larger forecast errors on occasion.

Figures 4 and 5 present a series of wind vector RMS difference diagrams in the tropics. Figure 4 depicts 200-hPa wind vector RMS differences comparing the control to the various denial experiments for the tropical region (20°N–20°S). The left column of Fig. 4 shows the January–February 2003 results while the right column shows the August–September 2003 results. Again, the results show the importance of AMSU data, which provide the largest impact. The rawinsonde data in January–February provide the next largest impact. Figure 5 depicts the 850-hPa wind vector RMS difference curves for days 0–7 for the control and five denial experiments in the tropical belt. The January–February 2003 results are in the left columns of Fig. 5 while the August–September 2003 results are in the right columns. The wind vector RMS difference was chosen as the tropical diagnostic since the variance of the anomaly correlation for 500-hPa geopotential height is very small in the tropics.

The error growth for both the 200-hPa vector RMS difference (Fig. 4) and the 850-hPa vector RMS difference (Fig. 5) is rapid during the first day, then slows as the integration proceeds. This tropical error characteristic is common in the GFS and other models as explained by Surgi (1989) and Surgi et al. (1998). These results are also consistent with those of Zapotocny et al. (2007).

This tropical comparison of vector RMS difference also identifies that the only data type to provide appreciable improvement to the forecasts during both time periods is the AMSU data type (see Figs. 4a and 4b and 5a and 5b). Rawinsondes provide some forecast improvement during the January–February time period (Fig. 4g), but very little improvement during August–September (Fig. 4h). The GEO winds provide a small negative impact to forecasts shorter than 2 days in length at 850 hPa during August–September (Fig. 5f), even though they will be shown to be very important to forecasting tropical cyclone positions on the 1–4-day time scale. These results are inconsistent with the assimilation experiments of Su et al. (2003). Su et al. (2003) found the Geostationary Operational Environmental Satellite (GOES) AMVs to have a negligible impact on the midlatitude 500-hPa geopotential height forecast skill but a slight positive impact on the tropical winds forecast. The remaining data types provide close to neutral impacts during both seasons for all forecasts out to 7 days.

Figures 6 and 7 present the polar region (60°–90°) 500-hPa geopotential height day-0–7 anomaly correlations for January–February and August–September 2003, respectively. Consistent with most results presented in this manuscript, the inclusion of AMSU data provides a higher anomaly correlation in the polar region during both seasons in each hemisphere (Figs. 6a–b and 7a–b). Also consistent with earlier results is that the Southern Hemisphere improvement from

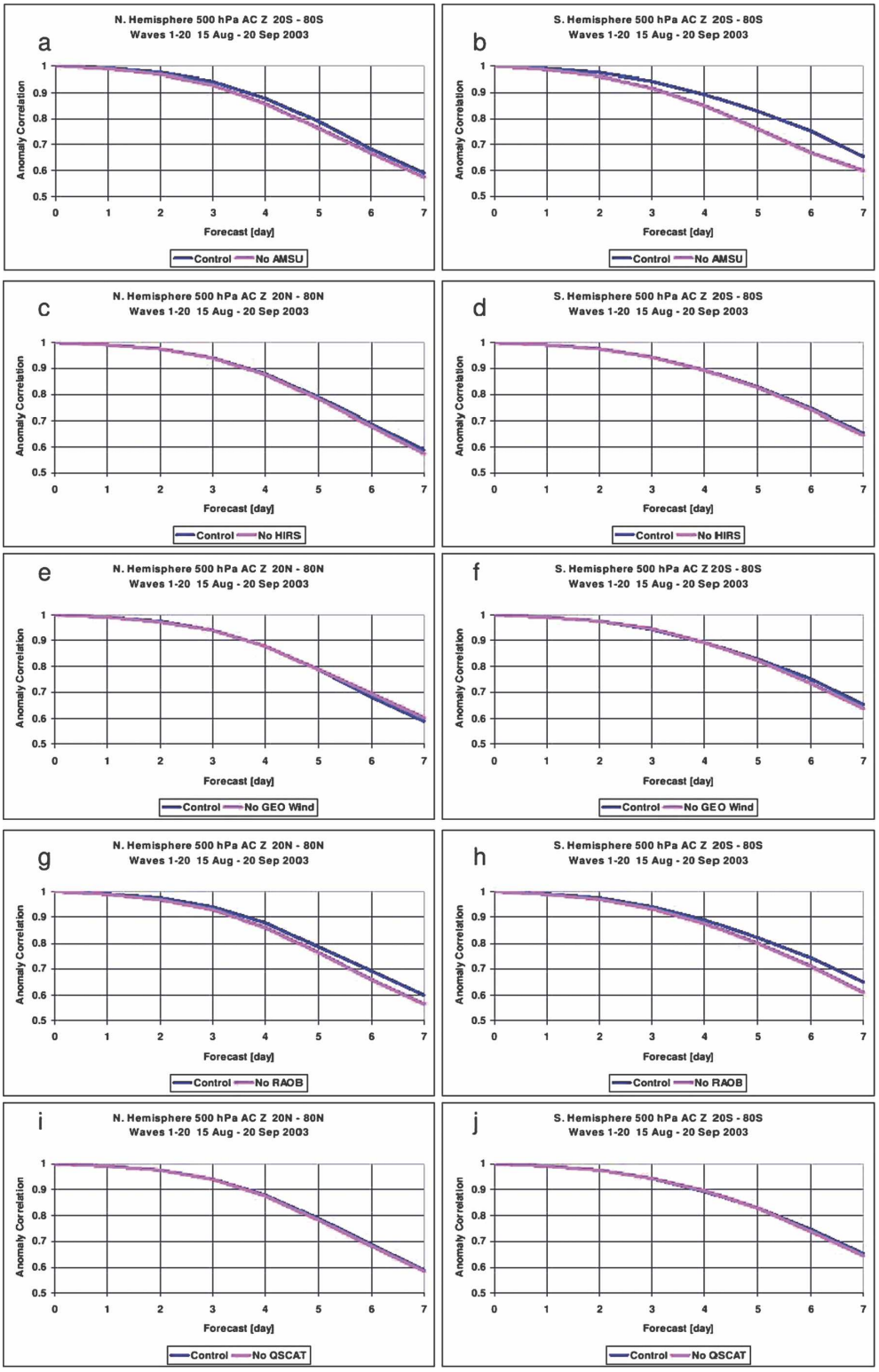

FIG. 3. The 15 Aug–20 Sep 2003 day-0–7 500-hPa geopotential height die-off curves for the control and five denial experiments. Shown are the (left) Northern Hemisphere and (right) Southern Hemisphere results.

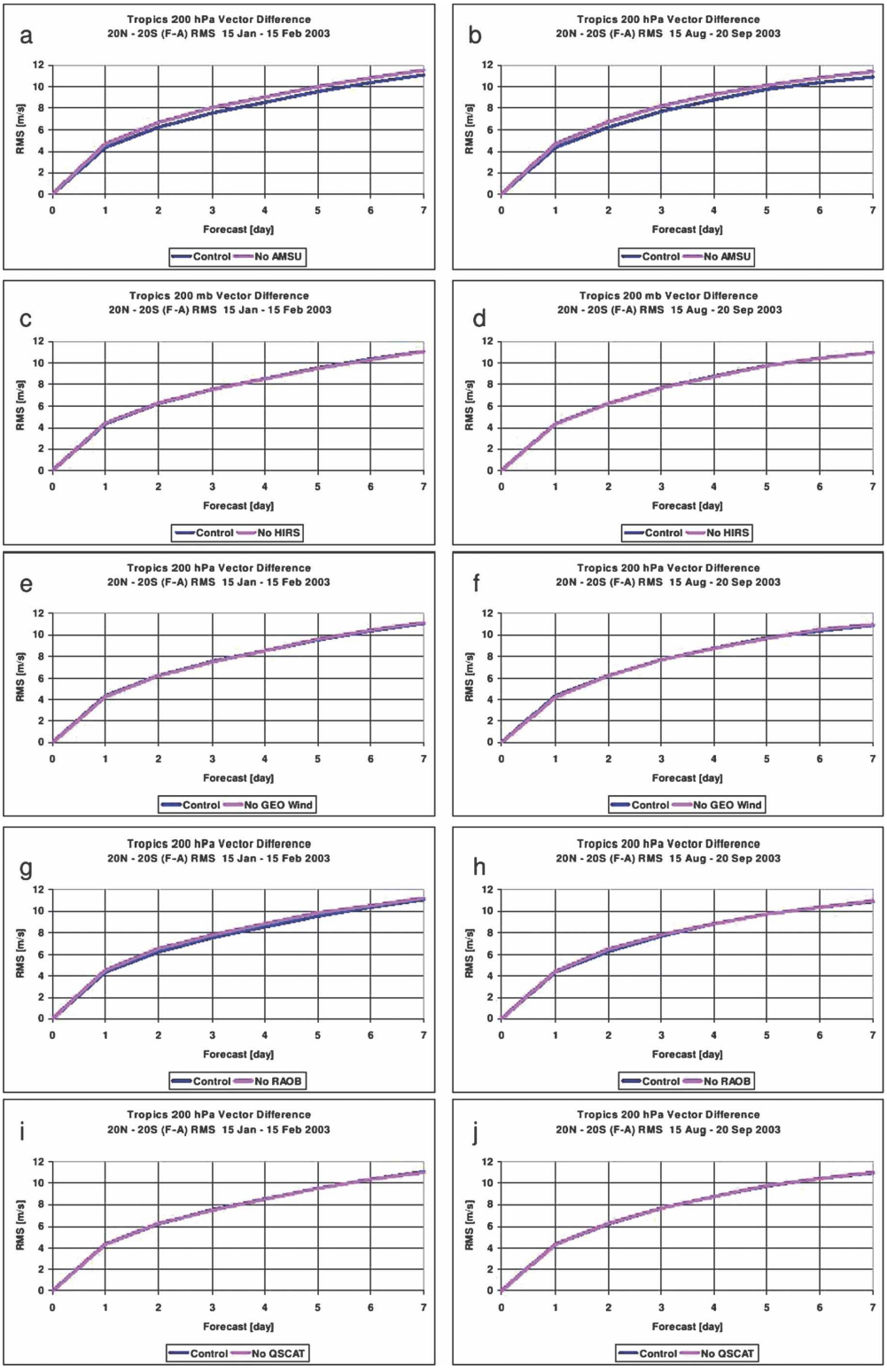

FIG. 4. The tropical 200-hPa day-0–7 RMS vector differences for the control and five denial experiments. Shown are the (left) 15 Jan–15 Feb 2003 and (right) 15 Aug–20 Sep 2003 results.

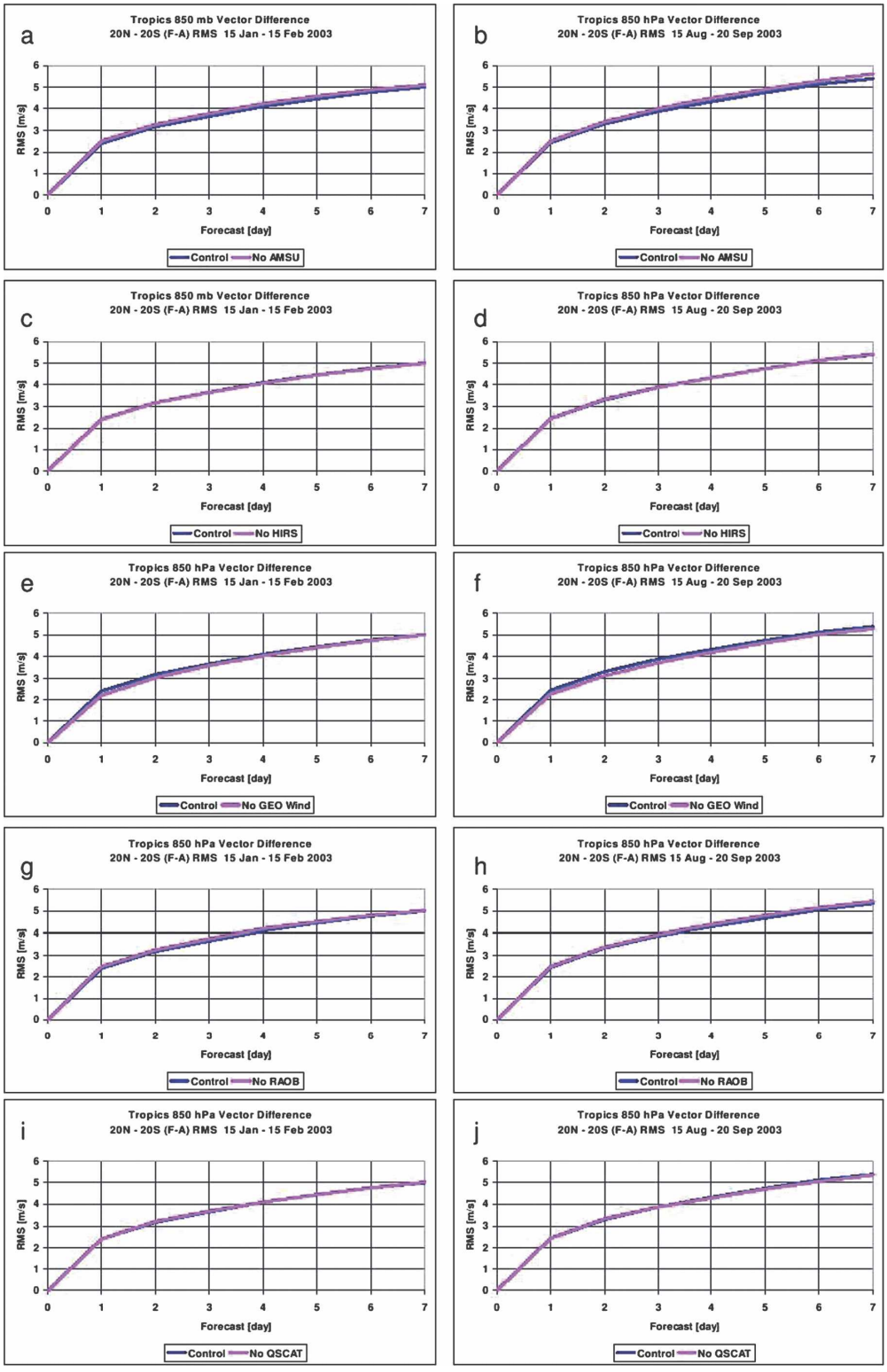

FIG. 5. The tropical 850-hPa day-0–7 RMS vector differences for the control and five denial experiments. Shown are the (left) 15 Jan–15 Feb 2003 and (right) 15 Aug–20 Sep 2003 results.

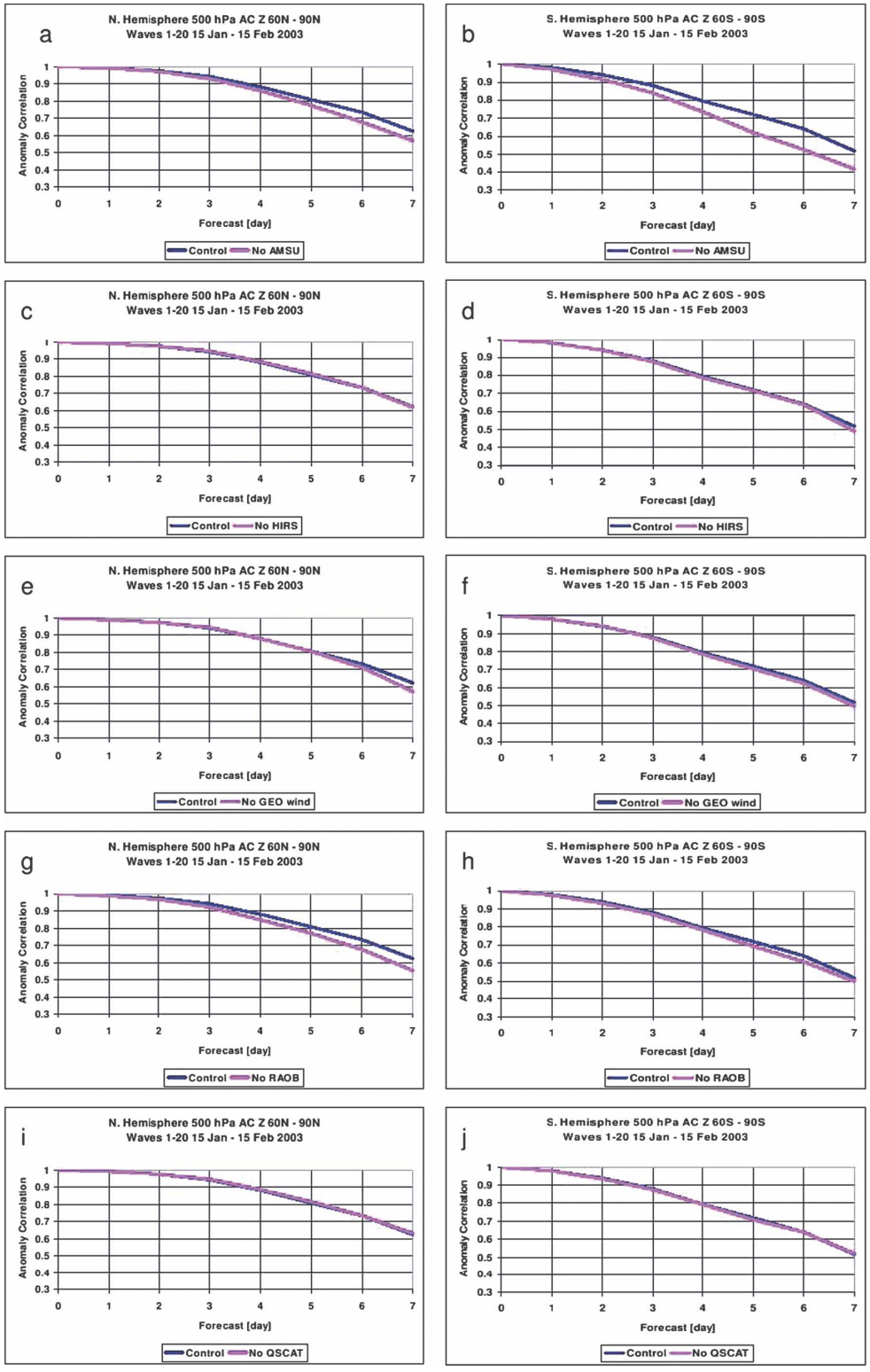

FIG. 6. The 15 Jan–15 Feb 2003 polar cap 500-hPa geopotential height day-0–7 anomaly correlation die-off curves for the control and five denial experiments. Shown are the (left) 60°–90°N and (right) 60°–90°S results.

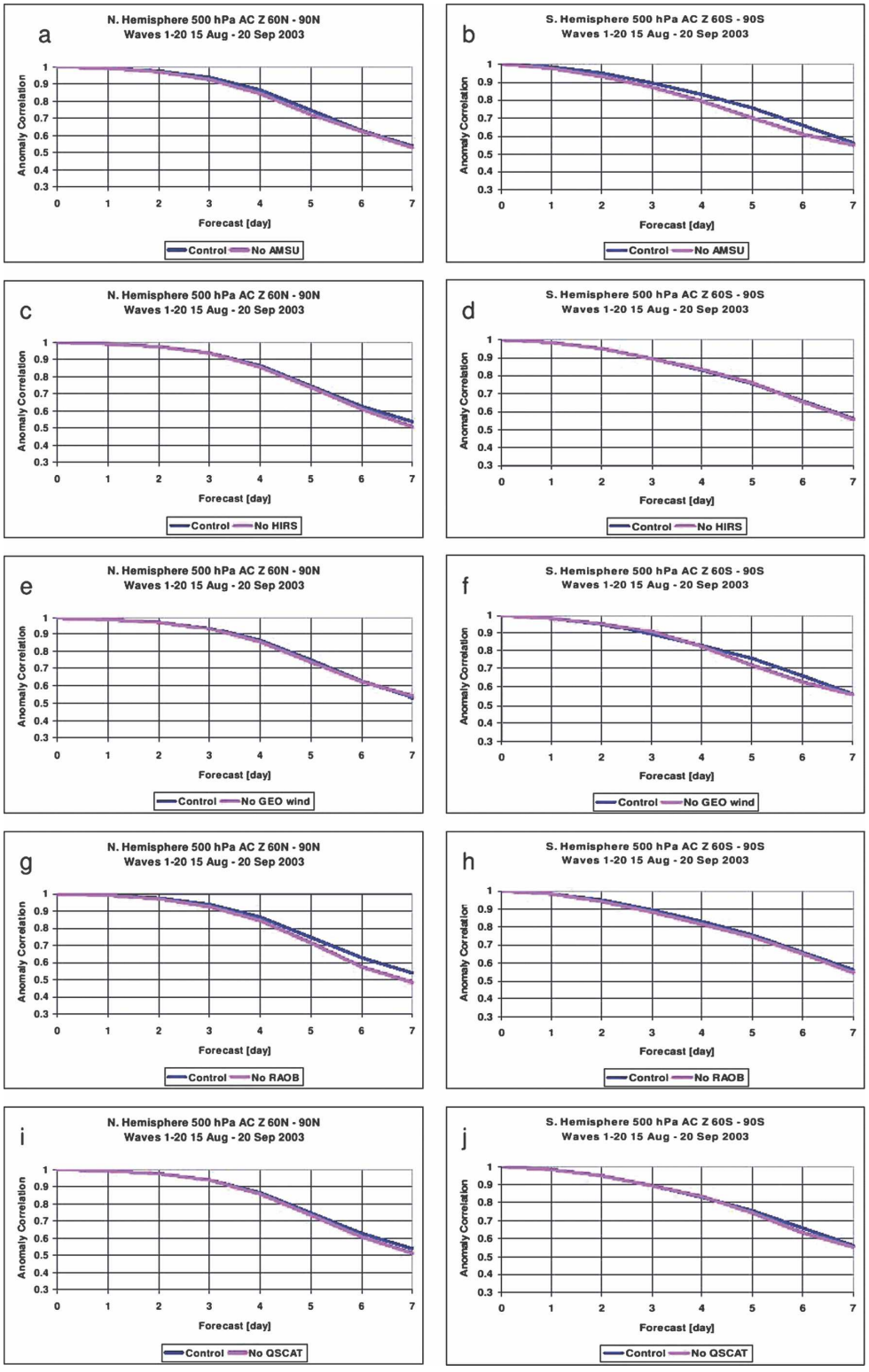

FIG. 7. The 15 Aug–20 Sep 2003 polar region 500-hPa geopotential height day-0–7 anomaly correlation die-off curves for the control and five denial experiments. Shown are the (left) 60°–90°N and (right) 60°–90°S results.

AMSU data is more dramatic than the Northern Hemisphere for these high-latitude regions.

An increased anomaly correlation is also seen with the inclusion of rawinsondes during both seasons and in each hemisphere (Figs. 6g–h and 7–h). The rawinsonde impact is greatest in the Northern Hemisphere during both seasons. This is probably because of the number of observations. There are more rawinsonde observations poleward of 60°N than there are poleward of 60°S.

The remaining data types provide a small positive impact in both hemispheres and seasons. This is expected for the GEO winds and QuikSCAT winds. The GEO winds are only derived at latitudes equatorward of 60° and over ocean. QuikSCAT surface winds are only generated over the ocean and under ice-free conditions. They still result in modest forecast improvements over the polar regions through the assimilation process.

b. Geographic distributions of forecast impact

In addition to the anomaly correlation statistics presented above, Figs. 8–12 present geographical distributions of the forecast impact for 500-hPa geopotential heights during the January–February and August–September 2003 time periods from all five denials investigated in this study. The figures are computed using (1) and present time-averaged forecast impacts for forecast hours 12, 24, 48, and 72. In these figures, negative forecast impacts have magenta shading, neutral or nearly neutral forecast impacts are not shaded, and positive forecast impact shadings proceed from blue to red.

Figures 8–12 present the five denials for both seasons. The AMSU denial results are shown in Fig. 8, the HIRS denial results are shown in Fig. 9, the GEO wind denial results are shown in Fig. 10, the rawinsondes denial results are shown in Fig. 11, and the QuikSCAT denial results are shown in Fig. 12.

The AMSU 12–72-h forecast impact results for January–February 2003 are shown in Figs. 8a–d, respectively. The 12-h results show that the largest forecast impacts are in the polar latitudes of each hemisphere with an equatorward extension of positive forecast impacts over the southern oceans and northern Pacific Ocean. High-latitude forecast impact results are between 150% and 200% with values steadily decreasing toward lower latitudes where very small negative forecast impacts are diagnosed within 20° of the equator. Forecast impacts greater than 100% are possible from (1) if the control and analysis fields are very similar. This results in dividing by a small denominator in (1).

Upon examining the 24–72-h forecast impacts (Figs. 8b–d), one notices a very steady decrease in the magnitude of the forecast impacts. In fact, by 72 h the largest forecast impacts are approximately 120% along 60°S with large regions of the globe being covered with neutral impacts (white regions). This decrease in forecast impact is consistent with the satellite data denial results of Zapotocny et al. (2007).

Figures 8e–h present the 500-hPa geopotential height AMSU denial forecast impact results for forecast hours 12–72 during August–September 2003. Comparing these results with the January–February 2003 results of Figs. 8a–d reveals that the forecast impact is much smaller for all time periods during August–September 2003 than during January–February 2003. In fact, by 72 h most of the globe is covered by neutral forecast impacts, with only scattered regions of small positive/negative impacts. These AMSU forecast impact results are consistent with the AMSU anomaly correlation results shown in Figs. 2 and 3. The largest day-3 Southern Hemisphere anomaly correlation improvements are noticed in the January–February time period with smaller improvements noticed in the August–September time period (cf. Figs. 2b and 3b at day 3). Similarly the largest day-3 forecast impacts are diagnosed during January 2003 in the 20°–80°S zonal band (cf. Figs. 8b and 8f). Recall that the geographic results in this section only extend to 3 days, while the anomaly correlation plots in section 4a extend to 7 days.

Consistent with all other results presented herein, the HIRS denial experiment provides very little forecast impact during either season in Fig. 9. This is true over almost the entire globe for all forecast hours from 12 to 72. Most positive–negative forecast impacts are primarily found at lower latitudes in oceanic regions.

The GEO wind denial results are more interesting, with large 12- and 24-h positive and negative forecast impacts diagnosed in the oceanic regions of the tropics and mostly the Northern Hemisphere during each season (Figs. 10–b and 10–f). During January–February 2003 the largest negative impacts are just west of South America and over the Mediterranean Sea and the Middle East (Fig. 10a). The 12- and 24-h negatives are not as large during August–September 2003 and are diagnosed over Russia and the region near Central America and northern South America (Figs. 10e and 10f). As with all other data types, these positive and negative forecast impacts early in the forecast cycle disappear with time such that by 72 h (Figs. 10d and 10h) generally weaker positive/negative forecast impacts are found within a field of largely neutral impacts.

The rawinsonde geographical forecast impact results (Fig. 11) are routinely the second largest of the five denials examined here. Similar to the AMSU forecast impact results of Fig. 8, the rawinsonde January–February 2003 forecast impacts are largest in polar regions,

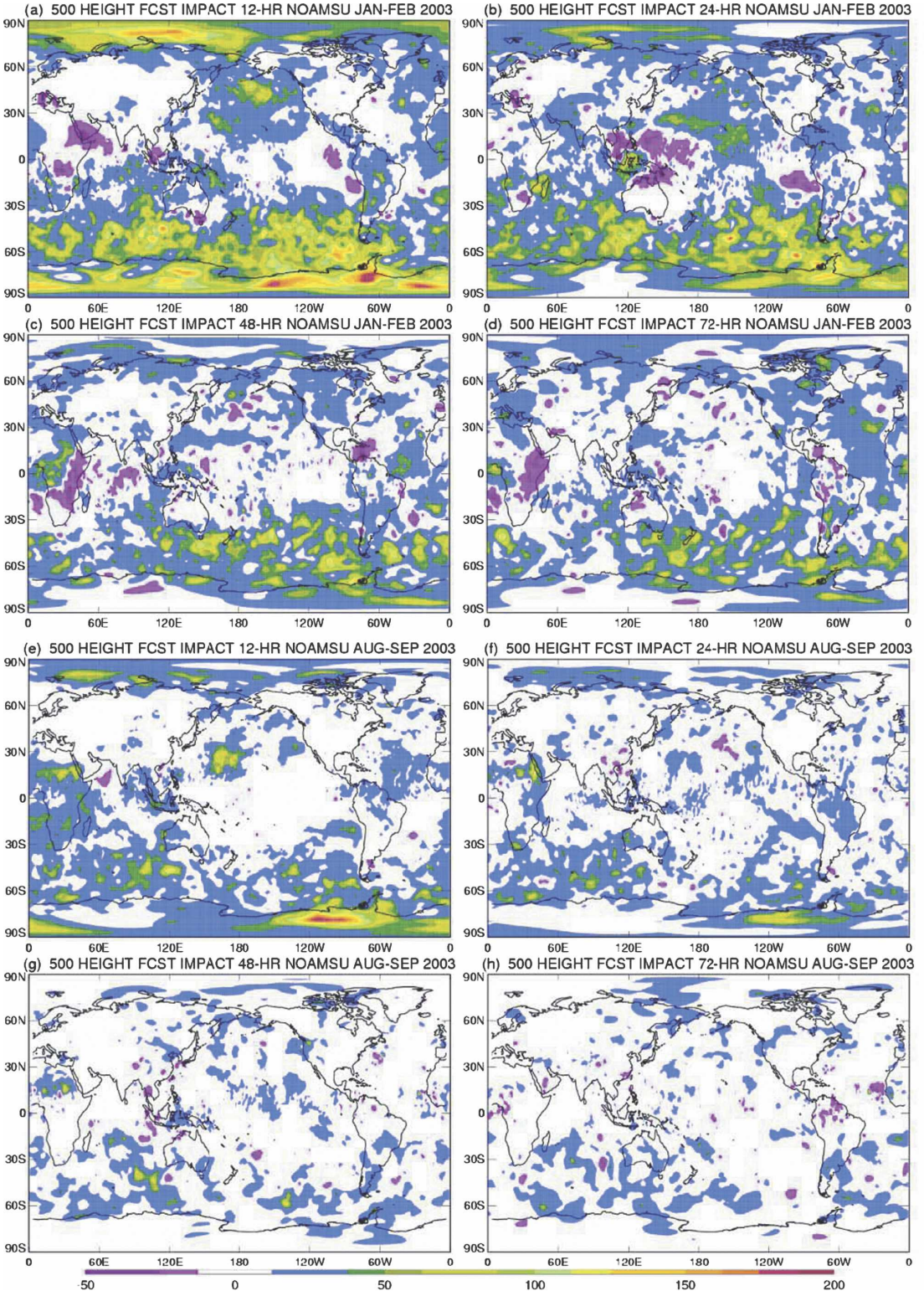

FIG. 8. Geographic distribution of the forecast impact to 500-hPa geopotential height from the denial of AMSU data during (top panels) January–February 2003 and (bottom panels) August–September 2003. The 12-, 24-, 48-, and 72-h impacts are shown for each time period with a color contour interval of 12.5%. Values within 12.5% of zero are white.

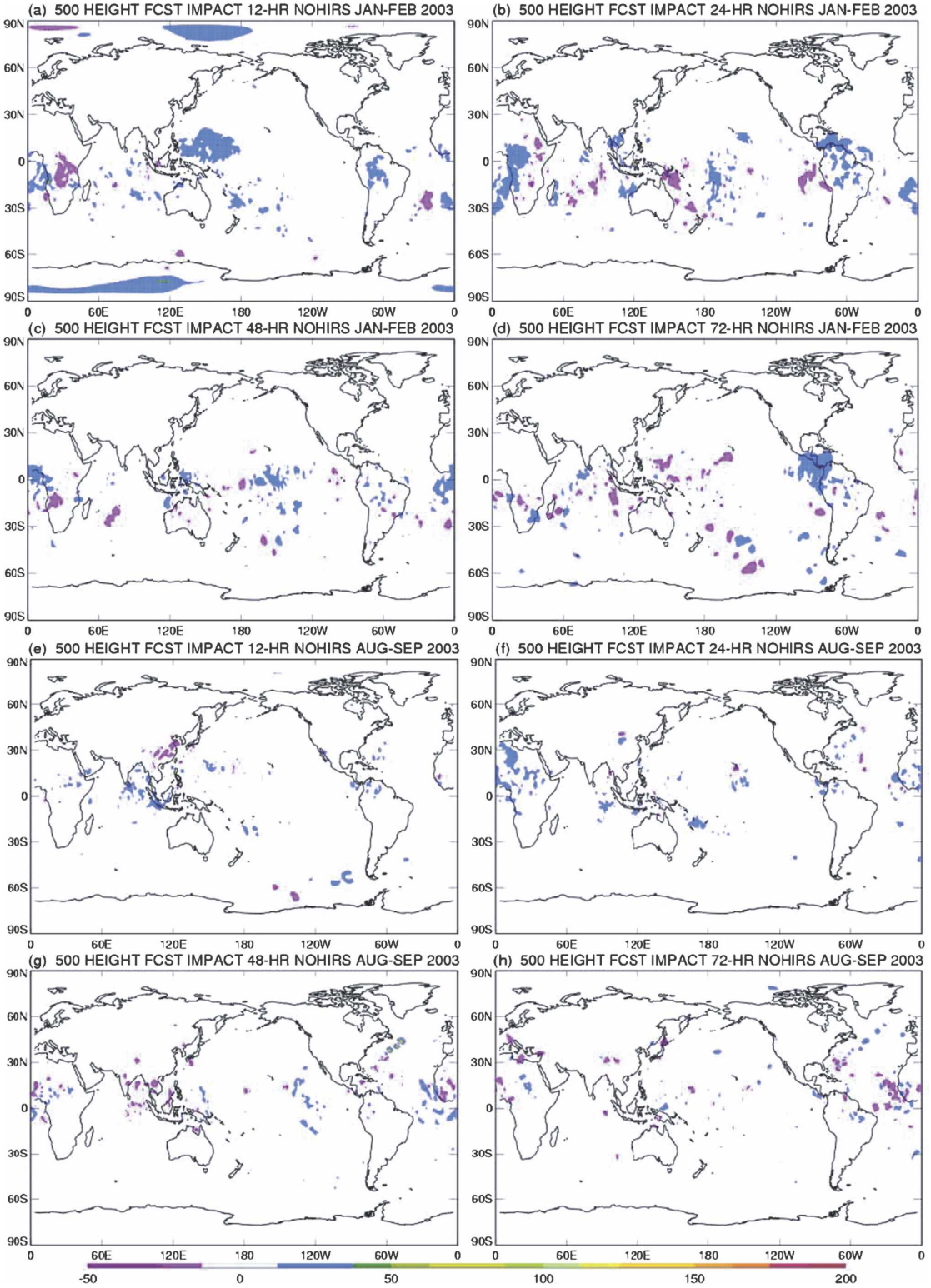

FIG. 9. Geographic distribution of forecast impact to 500-hPa geopotential height from the denial of HIRS data during (top panels) January–February 2003 and (bottom panels) August–September 2003. The 12-, 24-, 48-, and 72-h impacts are shown for each time period with color contour intervals of 12.5%. Values within 12.5% of zero are white.

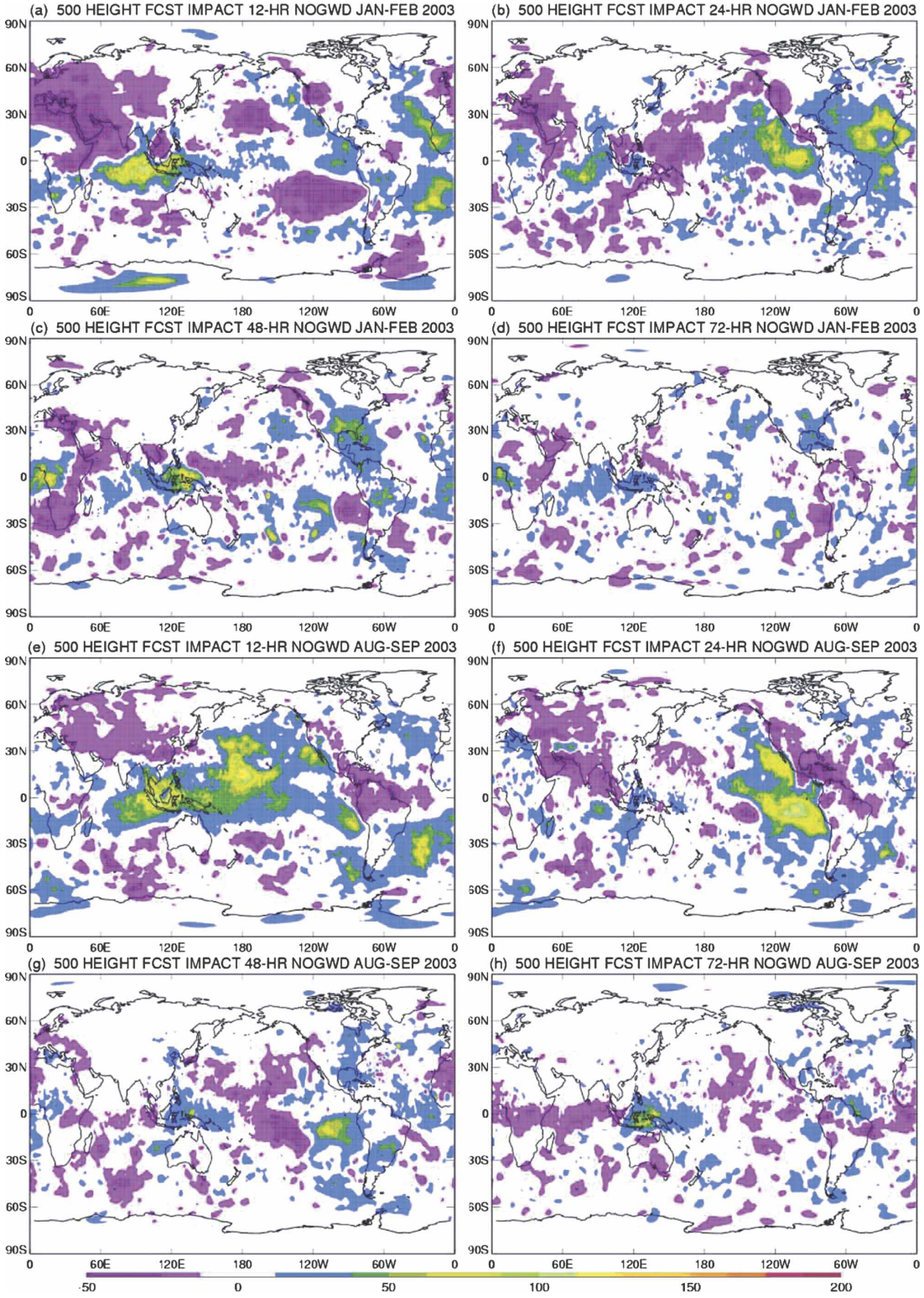

FIG. 10. Geographic distribution of forecast impact to 500-hPa geopotential height from the denial of GEO wind data during (top panels) January–February 2003 and (bottom panels) August–September 2003. The 12-, 24-, 48-, and 72-h impacts are shown for each time period with color contour intervals of 12.5%. Values within 12.5% of zero are white.

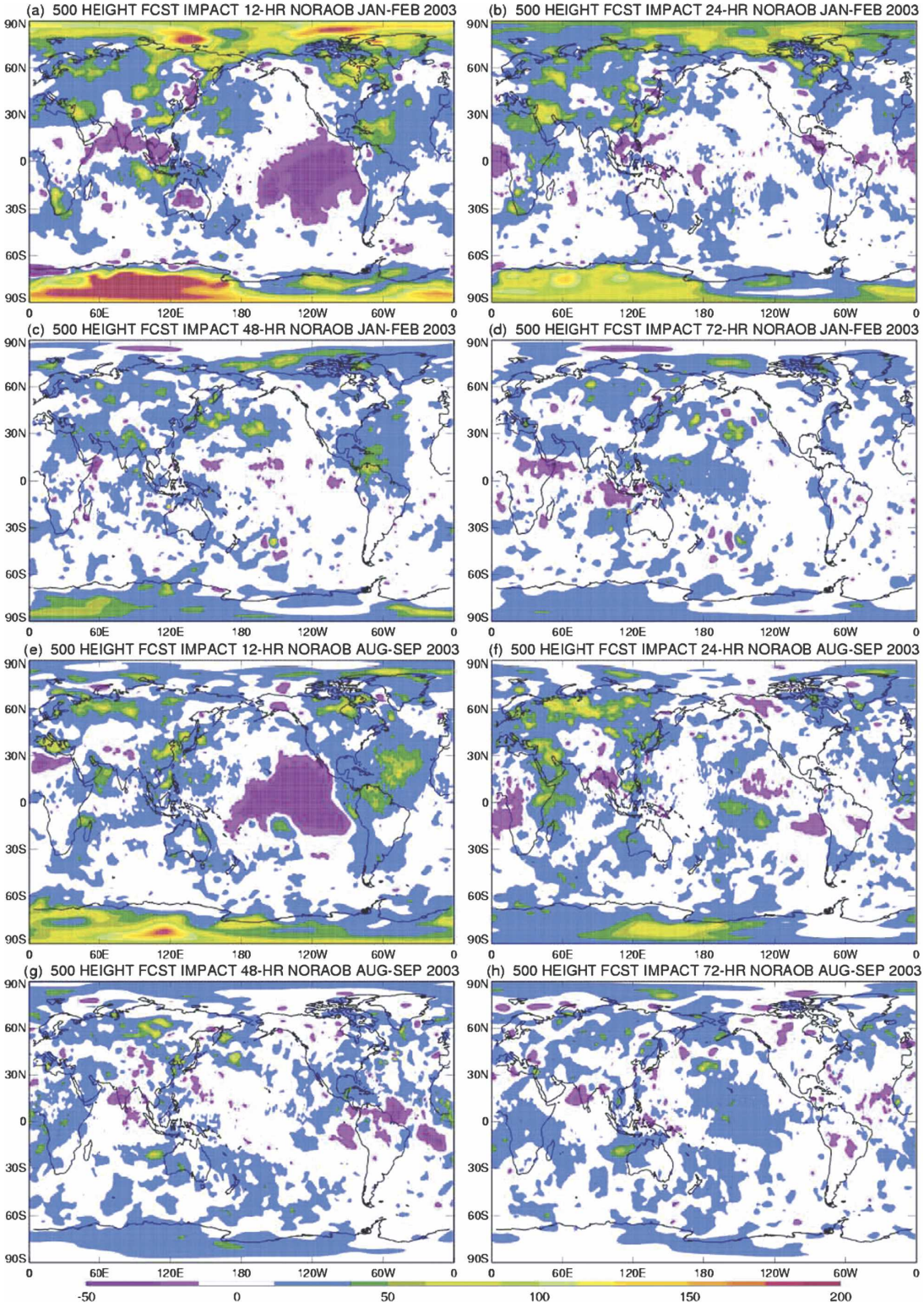

FIG. 11. Geographic distribution of forecast impact to 500-hPa geopotential height from the denial of raob data during (top panels) January–February 2003 and (bottom panels) August–September 2003. The 12-, 24-, 48-, and 72-h impacts are shown for each time period with color contours of interval 12.5%. Values within 12.5% of zero are white.

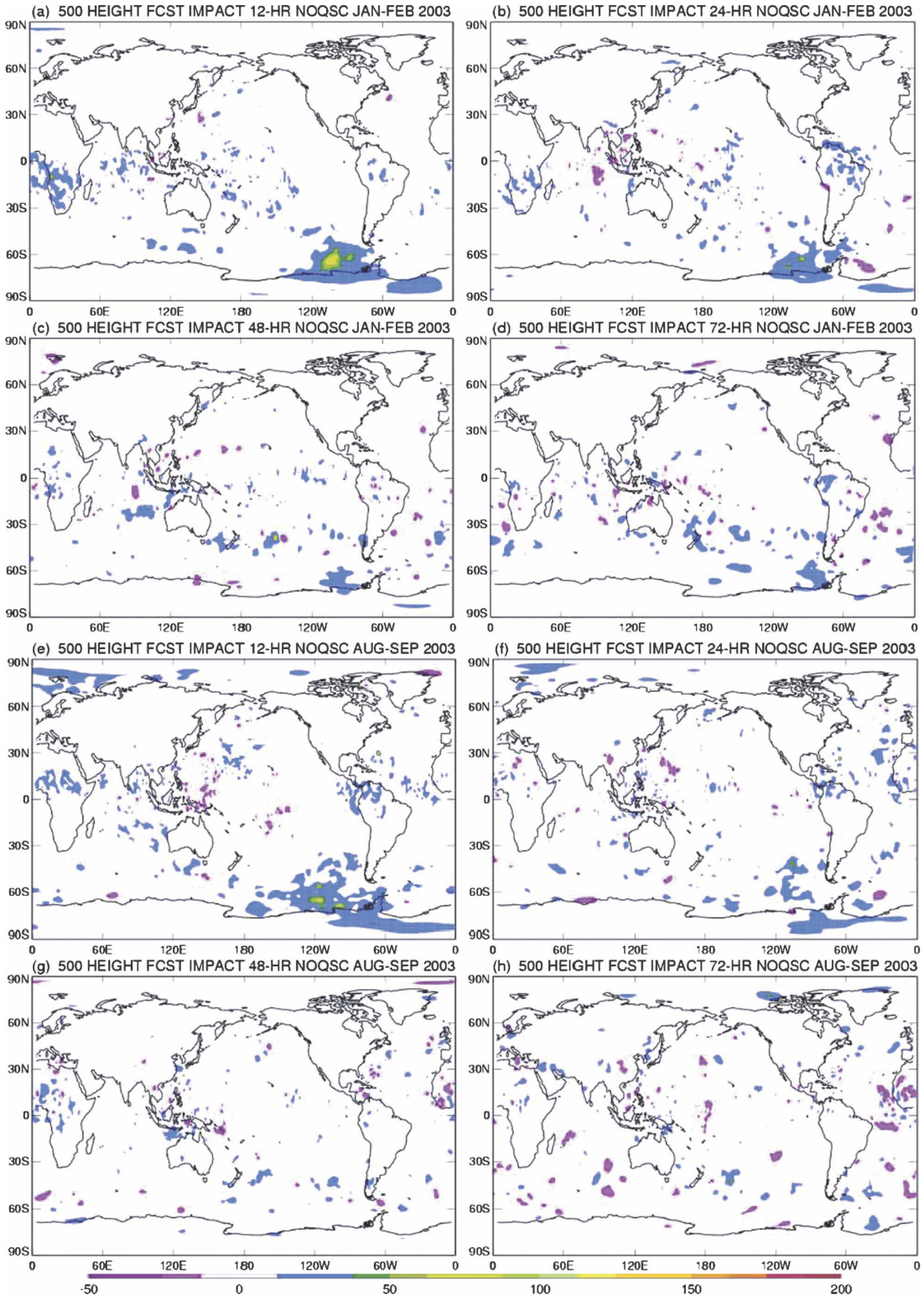

FIG. 12. Geographic distribution of forecast impact to 500-hPa geopotential height from the denial of QuikSCAT data during (top panels) January–February 2003 and (bottom panels) August–September 2003. The 12-, 24-, 48-, and 72-h impacts are shown for each time period with color contours of interval 12.5%. Values within 12.5% of zero are white.

especially Antarctica, with a dramatic decrease as the forecast proceeds. Also similar to the AMSU results is that the January–February 2003 rawinsonde forecast impacts are generally larger than their August–September 2003 counterparts. The largest 12-h negative forecast impacts from rawinsondes are found west of South America during both the January–February (Fig. 11a) and August–September (Fig. 11e) time periods. These regions of negative forecast impact at 12 h dissipate very quickly with time.

The QuikSCAT January–February 2003 and August–September 2003 forecast impact denial results are presented in Fig. 12. As with the HIRS results of Fig. 9, only small regions of the globe demonstrate positive/negative impacts. This is consistent with the anomaly correlation results presented above and is an expected result since QuikSCAT provides surface or near-surface winds to the assimilation system and the results presented here are for 500-hPa geopotential heights. They are nevertheless important for positioning synoptic systems and tropical cyclone track predictions (see section 4c.).

c. *Impact of removing selected satellite data on tropical cyclone track forecasts*

An important aspect of satellite data is to provide high-resolution temporal and spatial data in oceanic regions. This high volume of maritime data has the ability to greatly improve hurricane track forecasts both in the short term, before the storm system reaches the in situ data network over land, and in the longer term by more accurately resolving the steering currents while the system is far from land. This section examines the impact that removing four satellite data types has on hurricane track forecasts in both the Atlantic and eastern Pacific basins for 15 August–20 September 2003. All data used in the GFS were applied except for the specific data type denied in each experiment. The dropsondes in and around the hurricanes are included in all of these experiments. The operational NCEP vortex relocation algorithm, described by Lord (1991) and Liu et al. (2006), was also used. In order for a storm to be included in the diagnostics, the storm must exist in all of the experiments and the control. If a storm (tropical depression, tropical storm, or hurricane) is not found in one the experiments or the control, it is discarded from the statistics. These diagnostics are computed over only one season; as such, when interpreting these results, the number of storms must be considered. Results are not displayed for the eastern Pacific basin at 72 and 96 h because of a very small sample size.

The four data types investigated here are AMSU and HIRS radiances, winds from all geostationary satellites

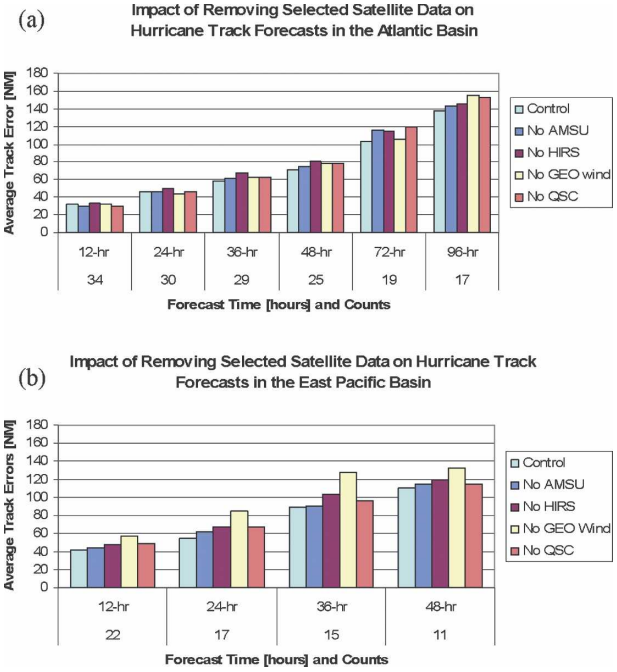

FIG. 13. Average track error (n mi) by forecast hour for the control simulation and experiments where AMSU, HIRS, GEO winds, and QuikSCAT were denied. Shown are the (a) Atlantic basin and (b) eastern Pacific basin results. A small sample size in the number of hurricanes precludes presenting the 72- and 96-h results in the eastern Pacific Ocean.

(GEO winds), and QuikSCAT low-level winds. Figure 13 displays the average track error in the GFS from the control simulation and where the four satellite data types have been denied. Inspection of Fig. 13 reveals that the average track error grows in the Atlantic basin (Fig. 13a) as time increases from about 30 n mi at 12 h to 145 n mi by 96 h. The same is true in the Pacific basin (Fig. 13b); however, in this diagnostic region the average error grows from near 50 n mi at 12 h to approximately 110 n mi at 48 h. For this season, the forecast degradation related to the removal of satellite observations in the Atlantic basin is seen in Fig. 13a. In general, the Atlantic basin storms are more accurately simulated by the GFS than are those in the Pacific basin. The results indicate for this study that denying an individual data type in the Atlantic basin often has less impact than in the Pacific basin. Possible explanations for these differences between basins include 1) more data upstream of the storms, 2) information from dropsondes being assimilated in the vicinity of Atlantic storms but not in the Pacific, and 3) reconnaissance flights that are also routinely conducted in and around Atlantic storms but not in the Pacific.

In the Pacific basin the track error is clearly larger from 12 to 48 h when the GEO winds are removed from

the analysis. Goerss and Hogan (2006) also found that the GEO winds had the greatest impact on hurricane track error in the Navy Operational Global Atmospheric Prediction System. The remaining three data types (AMSU, HIRS, and QuikSCAT) produce almost similar track errors between themselves and the control simulations in the eastern Pacific basin. An interesting difference between the results of this section and the results presented in section 4a is that the Pacific basin tropical cyclone storm tracks are clearly degraded from the removal of GEO winds data through 48 h while the August–September day-5 tropical 850-hPa vector difference RMSs were lower when the GEO winds were removed.

5. Summary

This paper has quantified the contributions to forecast accuracy made by conventional rawinsonde data and four remotely sensed satellite data types. This work was done by using OSEs and examining the 0–168-h forecast impact results in NCEP's Global Data Assimilation System and the Global Forecast System during January–February and August–September 2003.

The results show that the AMSU and rawinsonde data provide the largest increase in forecast quality in the polar, midlatitude, and tropical regions. Much smaller improvements to the anomaly correlation are realized from the inclusion of the other data types. However, it is important to note that no data type provides an overall negative impact in the 20°–80° zonal bands of each hemisphere.

The 500-hPa geopotential height geographic distributions of forecast impact shown in Figs. 8–12 also indicate that AMSU radiances and rawinsonde data provide the largest impact. In general, their largest impacts are found in polar latitudes and in the zonal belts of 20°–80° in each hemisphere. Several of the data types provide some negative forecast impacts in the tropical regions, especially just west of South America. All data types also display a rapid decrease in forecast impact globally as the simulations proceed from 12 to 72 h.

In contrast to the anomaly correlations and geographical forecast impact results, where AMSU and rawinsondes data routinely provided the largest gain to forecast quality, the geostationary wind data aided tropical cyclone track forecasts in the eastern Pacific basin the most. In this region the track errors are approximately 45 n mi worse at 36 h when removing the geostationary data (see Fig. 13b). In the Atlantic basin all satellite data types provide a nearly equal contribution to the tropical cyclone forecast track quality.

This work is being extended to include assessing the impact of removing one and two NOAA polar-orbiting satellites from the current suite of three in the operational assimilation system. Another project is investigating improved quality control procedures for the GEO winds (Le Marshall et al. 2004a,b) in NCEP's assimilation system. Other projects include a detailed examination of the impacts in the NCEP Gridpoint Statistical Interpolation (GSI) system (which will replace the currently operational SSI) from AMV data from the MODIS, AIRS radiances, ocean surface wind vector measurements from space using *WINDSAT*, and the effective exploitation of new hyperspectral data, which will become available from the Infrared Atmospheric Sounding Interferometer (IASI), the Cross-track Infrared Sounder (CrIS), the Geosynchronous Imaging Fourier Transform Spectrometer (GIFTS), and GOES-R instruments.

Acknowledgments. The authors thank Stephen Lord, Dennis Keyser, Stacie Bender, and John Derber of NCEP for providing the appropriate hardware–software support and guidance. The authors also thank Timothy J. Schmit of NOAA/NESDIS/ORA for his enlightening scientific input and Qingfu Liu for his help with the hurricane track statistics. The study was undertaken within the Joint Center for Satellite Data Assimilation (JCSDA) and supported under NOAA Grant NA07EC0676, which supports Joint Center activities.

REFERENCES

Alishouse, J. C., S. Snyder, J. Vongsathorn, and R. R. Ferraro, 1990: Determination of oceanic total precipitable water from the SSM/I. *IEEE Trans. Geosci. Remote Sens.,* **28,** 811–816.

Derber, J. C., D. F. Parrish, and S. J. Lord, 1991: The New Global Operational Analysis System at the National Meteorological Center. *Wea. Forecasting,* **6,** 538–547.

Goerss, J. S., and T. F. Hogan, 2006: Impact of satellite observations and forecast model improvements on tropical cyclone track forecasts. Preprints, *27th Conf. on Hurricanes and Tropical Meteorology,* Monterey, CA, Amer. Meteor. Soc., P5.2.

Kanamitsu, M., and Coauthors, 1991: Recent changes implemented into the Global Forecast System at NMC. *Wea. Forecasting,* **6,** 425–435.

Kelly, G., 1997: Influence of observations on the operational ECMWF system. *Tech. Proc. Ninth Int. TOVS Study Conf.,* Igls, Austria, Int. TOVS Working Group, 239–244.

Keyser, D., cited 2001a: Code table for PREPBUFR report types used by the ETA/3DVAR. [Available online at http://www.emc.ncep.noaa.gov/mmb/data_processing/prepbufr.doc/table_4.htm.]

——, cited 2001b: Summary of the current NCEP analysis system usage of data types that do not pass through PREPBUFR processing. [Available online at http://www.emc.ncep.noaa.gov/mmb/data_processing/prepbufr.doc/table_19.htm.]

——, cited 2003: Observational data processing at NCEP. [Available online at http://www.emc.ncep.noaa.gov/mmb/data_processing/.]

Kistler, R., and Coauthors, 2001: The NCEP–NCAR 50-Year Reanalysis: Monthly means CD-ROM and documentation. *Bull. Amer. Meteor. Soc.,* **82,** 247–267.

Lahoz, W. A., 1999: Predictive skill of the UKMO Unified Model in the lower stratosphere. *Quart. J. Roy. Meteor. Soc.,* **125,** 2205–2238.

Le Marshall, J., A. Rea, L. Leslie, R. Seecamp, and M. Dunn, 2004a: Error characterization of atmospheric motion vectors. *Aust. Meteor. Mag.,* **53,** 123–131.

——, R. Seecamp, J. Daniels, C. Velden, K. Puri, R. Bowen, A. Rea, and M. Dunn, 2004b: The contribution of *GOES-9* to operational NWP forecast skill in the Australian region. *Aust. Meteor. Mag.,* **53,** 279–283. [Available online at http://cimss.ssec.wisc.edu/itwg/itsc/itsc13/proceedings/session7/7_1_lemarshall.pdf.]

Liu, Q., S. Lord, N. Surgi, Y. Zhu, R. Wobus, Z. Toth, and T. Marchok, cited 2006: Hurricane relocation in Global Ensemble Forecast System. Preprints, *27th Conf. on Hurricanes and Tropical Meteorology,* Monterey, CA, Amer. Meteor. Soc., P5.13.

Lord, S. J., 1991: A bogussing system for vortex circulations in the National Meteorological Center Global Forecast Model. Preprints, *19th Conf. on Hurricane and Tropical Meteorology,* Miami, FL, Amer. Meteor. Soc., 329–330.

Menzel, W. P., F. C. Holt, T. J. Schmit, R. M. Aune, A. J. Schreiner, G. S. Wade, and D. G. Gray, 1998: Application of *GOES-8/9* soundings to weather forecasting and nowcasting. *Bull. Amer. Meteor. Soc.,* **79,** 2059–2077.

Miller, A. J., and Coauthors, 1997: Information content of Umkehr and SBUV(2) satellite data for ozone trends and solar responses in the stratosphere. *J. Geophys. Res.,* **102,** 19 257–19 263.

NOAA, cited 2005: NOAA Polar Orbiter Data (POD) user's guide, November 1998 revision. [Available online at http://www2.ncdc.noaa.gov/docs/klm/html/c3/sec3-3.htm.]

NWS, cited 2007: Model performance statistics. [Available online at http://wwwt.emc.ncep.noaa.gov/gmb/STATS/STATS.html.]

Parrish, D. F., and J. C. Derber, 1992: The National Meteorological Center's Spectral Statistical Interpolation Analysis System. *Mon. Wea. Rev.,* **120,** 1747–1763.

Reale, A. L., 1995: Departures between derived satellite soundings and numerical weather forecasts: Present and future. *Tech. Proc. Eighth Int. TOVS Study Conf.,* Queenstown, New Zealand, International TOVS Working Group, 395–404.

Smith, W. L., H. M. Woolf, C. M. Hayden, D. Q. Wark, and L. M. McMillin, 1979: The TIROS-N Operational Vertical Sounder. *Bull. Amer. Meteor. Soc.,* **60,** 1177–1187.

Spencer, R. W., and J. R. Christy, 1992: Precision and radiosonde validation of satellite gridpoint temperature anomalies. Part I: MSU channel 2. *J. Climate,* **5,** 847–857.

Su, X., J. Derber, S. Lord, C. Velden, and J. Daniels, 2003: Toward improved use of GOES satellite-derived winds at the National Centers for Environmental Prediction (NCEP). NCEP Office Note 440, 18 pp.

Surgi, N., 1989: Systematic errors of the FSU Global Spectral Model. *Mon. Wea. Rev.,* **117,** 1751–1766.

——, H.-L. Pan, and S. J. Lord, 1998: Improvement of the NCEP Global Model over the Tropics: An evaluation of model performance during the 1995 hurricane season. *Mon. Wea. Rev.,* **126,** 1287–1305.

Uppala, S. M., and Coauthors, 2005: The ERA-40 re-analysis. *Quart. J. Roy. Meteor. Soc.,* **131,** 2961–3012.

Velden, C. S., C. M. Hayden, S. J. Nieman, W. P. Menzel, S. Wanzong, and J. S. Goerss, 1997: Upper-tropospheric winds derived from geostationary satellite water vapor observations. *Bull. Amer. Meteor. Soc.,* **78,** 173–195.

WMO, 1999: Commission for basic systems abridged final report with resolutions and recommendations. Rep. WMO 893, 184 pp. [Available online at http://www.wmo.ch/pages/prog/www/CBS/Reports/CBS-Ext98_Karlsruhe1998/WMO-893_en.pdf.]

Yu, T.-W., and R. D. McPherson, 1984: Global data assimilation experiments with scatterometer winds from SEASAT-A. *Mon. Wea. Rev.,* **112,** 368–376.

Zapotocny, T. H., and Coauthors, 2000: A case study of the sensitivity of the Eta Data Assimilation System. *Wea. Forecasting,* **15,** 603–621.

——, W. P. Menzel, J. P. Nelson III, and J. A. Jung, 2002: An impact study of five remotely sensed and five in situ data types in the Eta Data Assimilation System. *Wea. Forecasting,* **17,** 263–285.

——, ——, J. A. Jung, and J. P. Nelson III, 2005a: A four-season impact study of rawinsonde, GOES, and POES data in the Eta Data Assimilation System. Part I: The total contribution. *Wea. Forecasting,* **20,** 161–177.

——, ——, ——, and ——, 2005b: A four-season impact study of rawinsonde, GOES, and POES data in the Eta Data Assimilation System. Part II: Contribution of the components. *Wea. Forecasting,* **20,** 178–198.

——, J. A. Jung, J. F. Le Marshall, and R. E. Treadon, 2007: A two-season impact study of satellite and in situ data in the NCEP Global Data Assimilation System. *Wea. Forecasting,* **22,** 887–909.